Variations in the extent and elevation of the Larsen A and B ice shelves, Antarctica, derived from multiple datasets

Jun Chen
Changqing Ke
Xiaobing Zhou

SPIE.

Variations in the extent and elevation of the Larsen A and B ice shelves, Antarctica, derived from multiple datasets

Jun Chen,[a,b,c] Changqing Ke,[a,b,]* and Xiaobing Zhou[d]

[a]Nanjing University, School of Geographic and Oceanographic Sciences, Nanjing, China
[b]Nanjing University, Jiangsu Provincial Key Laboratory of Geographic Information Science and Technology, Nanjing, China
[c]Anhui Jianzhu University, School of Environment and Energy Engineering, Hefei, China
[d]Montana Tech of the University of Montana, Department of Geophysical Engineering, Butte, Montana, United States

Abstract. Accurate measurements of retreat and progressive lowering of ice shelves are critical for estimating the mass balance of the Antarctic ice sheet under projected warming. Ice shelf extent was extracted from declassified aerial photographs and modern satellite images (Landsat and Moderate Resolution Imaging Spectroradiometer imagery), and a 48-year time series of the areal extents of the Larsen A ice shelf (LAIS) and the Larsen B ice shelf (LBIS) was compiled. In addition, we characterize the surface elevation changes of the LAIS and LBIS over the last two decades by combining the Ocean Topography Experiment/Poseidon and the Envisat Radar Altimeter-2 using the collinear analysis method. The Larsen ice shelf displayed no significant changes until the late 1980s, whereas the LAIS has retreated rapidly since 1986, and the LBIS has followed a similar pattern since the early 1990s. The LAIS and LBIS have already diminished by ~14,000 km^2 in total since 1968. As the ice shelves retreated, the surface elevations of the LAIS and LBIS exhibited progressive lowering from 1992 to 2010, with the lowering rate of the LAIS significantly greater than that of the LBIS. The remaining ice of the LAIS was lowered at a rate of 0.45 $m\,a^{-1}$ from 1992 to 2001, and the remnant LBIS was lowered at a rate of 0.07 $m\,a^{-1}$ from 1992 to 2010. In response to the continuous retreat of the LAIS and LBIS, their surface elevations are very sensitive to the collapse and retreat of the ice shelves. © *2018 Society of Photo-Optical Instrumentation Engineers (SPIE)* [DOI: [10.1117/1.JRS.12.046019]]

Keywords: Larsen ice shelf; retreat; thinning; optical remote sensing images; radar altimetry; atmospheric warming.

1 Introduction

The Antarctic ice sheet is strongly affected by global climate change.[1] As global warming intensifies,[2] an ice shelf plays an increasingly important role as an amplifier and indicator of global climate changes.[3] The Larsen ice shelf (LIS) is an extensive area of floating glacier ice that borders the eastern side of the Antarctic Peninsula (AP). The mean air temperature in the AP has increased since the late 1940s by ~0.5°C per decade,[4] and the regional climate warming has led to longer melt seasons and increasingly extensive melt ponds over the LIS.[5] Meanwhile, the ocean temperature in the Weddell Sea has risen, increasing the rate of basal melting and thereby contributing to the collapse of the LIS.[6] The retreat of ice shelves on the AP over the past decades is well documented and has been attributed to atmospheric and oceanic warming.[7] In short, the LIS has become a popular location for studies of global warming.

The gradual retreat of the LIS has been interrupted by three calving events, specifically, the disintegration of the Larsen A ice shelf (LAIS) in January 1995, which was accompanied

---

*Address all correspondence to: Changqing Ke, E-mail: kecq@nju.edu.cn

by a loss of ~1600 km^2 of floating ice; the disintegration of the Larsen B ice shelf (LBIS) in February to March 2002, which was accompanied by a loss of ~3250 km^2 of floating ice;[8] and a calving event in the Larsen C ice shelf (LCIS) in July 2017.[9] The retreat or disappearance of the LAIS and the LBIS may have led to a reduction in backstress, producing accelerated ice flow and surface elevation lowering. The elevation reduction is an indicator of mass loss, and the LAIS and the LBIS have shown significant elevation reductions and large negative mass imbalances.[10] In summary, accurate information on the retreat and progressive thinning of ice shelves is critical in the assessment of ice sheet mass balance under projected global warming.

The front locations of the LIS have been tracked since 1940s by field observations; the global positioning system is the main tool that has been used to monitor changes in the ice extent and elevation of the Antarctic ice sheet in recent decades. However, field observations have substantial limitations, such as high costs, and they are collected in harsh environments. Remote sensing has been widely used in monitoring the Antarctic ice sheet.[11,12] Aerial photography was the first method used to monitor changes in Antarctic ice. Declassified aerial photographs have very high spatial resolution, and some were taken at times well before the existence of satellite images. However, aerial photographs have several limitations. Declassified aerial photos are not continuous in time, the processing techniques applied to aerial photographs are scarce and complex, and the geolocation accuracy is not guaranteed. Satellite optical images are presently the main tool used to monitor ice shelf extent, and synthetic aperture radar (SAR) images supplement these optical images.[13,14]

Ice sheet surface elevation changes can also be retrieved using remote sensing. Satellite stereoimage digital elevation model differencing (dDEM)[15] is a valuable technique for detecting elevation changes,[16] whereas SAR interferometry has higher accuracy than the dDEM technique. In addition, satellite altimetry has been widely applied to detect changes in the surface elevations of ice shelves, along with other geodetic methods.[17,18] Satellite altimetry is mainly classified into two categories, such as laser altimetry and radar altimetry. Laser altimetry has a much smaller footprint size than radar altimetry and is thus more suitable for assessing elevation changes over mountain glaciers with rough terrain and steep slopes. However, in the open areas of Antarctic ice shelves, which display limited topographic variability,[19] radar altimetry can still achieve satisfactory results despite its larger footprint size.

Four methods can be used to retrieve elevation differences based on radar altimetry data: (1) geometrically overlapping footprint pairs,[20] (2) crossover analysis,[21] (3) collinear (repeat-track) analysis,[22] and (4) collinear analysis with the help of DEMs.[23] The geometrically overlapping footprint pairs and crossover analysis methods may not be suitable for accurate monitoring of elevation changes due to the small areas of the LAIS and the LBIS. In addition, the Advanced Spaceborne Thermal Emission and Reflection Radiometer Global Digital Elevation Model has large errors in this region. Cook et al.[24] generated a new DEM that covers only grounded ice and masks out the ice shelves. The collinear analysis method is useful over small study regions, where few crossover locations can be found.

Previous studies of the surface elevation changes in the LIS have focused on the LCIS because its extent has remained relatively stable in recent decades.[25] However, the LAIS and the LBIS have either retreated significantly or been almost entirely lost. Thus, most researchers have excluded the LAIS from their surface elevation monitoring and studies, and few detailed analyses of the elevation changes of the LBIS have been performed. Therefore, this study examined the surface elevation changes in both the LAIS and the LBIS over the last two decades. We employed the collinear analysis method to retrieve the ice surface elevation changes using data collected by the Ocean Topography Experiment/Poseidon (T/P) and the Envisat Radar Altimeter-2 (RA-2). Additionally, we compiled a 48-year time series of monitoring data for studying the retreat of the LAIS and LBIS by combining declassified aerial photographs and satellite images [Landsat and Moderate Resolution Imaging Spectroradiometer (MODIS) imagery]. Based on the above sources of information, we discuss the mechanisms underlying the observed changes in ice-shelf surface mass balance and the relationship between the retreat and progressive lowering of ice shelves in the context of atmospheric warming.

2 Study Area, Data, and Methodology

2.1 *Study Area*

The LIS is a series of shelves that occupy distinct embayments along the northeast coast of the AP, and the segments from north to south are called the Larsen A, B, C, and D ice shelves (Fig. 1). The study area mainly covers the LAIS and the LBIS, which are located on the eastern side of the Oscar II Coast. The northern LIS is confined by the Longing and Sobral Peninsulas to the north and extends to the Jason Peninsula. The Seal Nunataks and Robertson Island divide the study area into the LAIS and the LBIS.
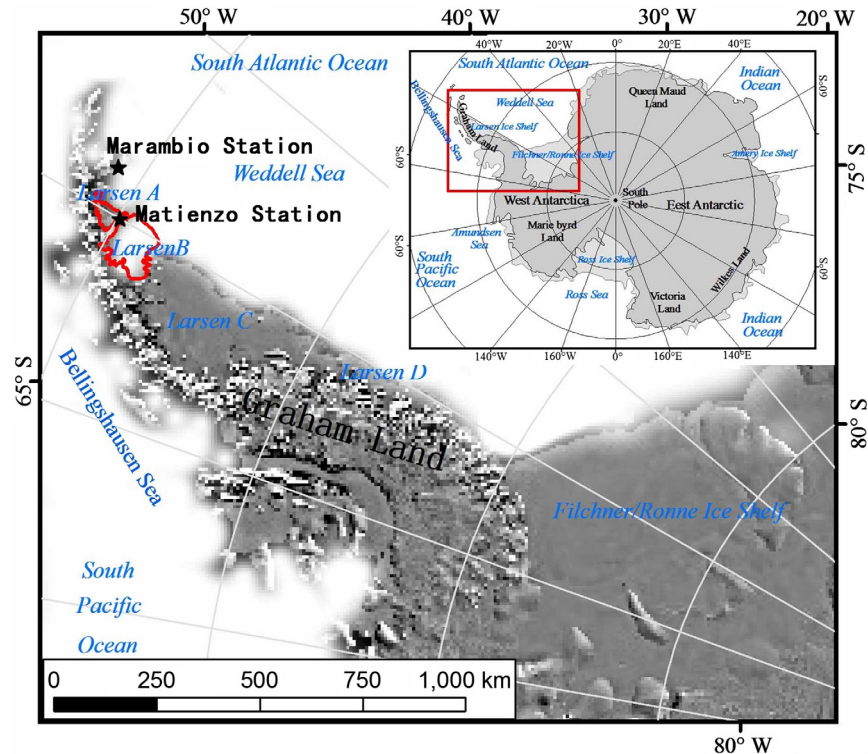

Fig. 1 Locations of the Larsen ice shelves in the AP. The underlying image is the MODIS mosaic from Haran et al.[26] The position of the MODIS image is indicated by the red rectangle in the upper-right inset.

Table 1 Specifications of the ASFR photos used to locate the ice shelf front.

Flight line ID	Flight date	Photographic frame
2159	December 27, 1968	228
2143	December 24, 1968	414
2158	December 27, 1968	126
1353	September 26, 1968	264
2152	December 27, 1968	240
2147	December 21, 1968	186
2157	December 27, 1968	207

2.2 Optical Images for Measuring Ice Shelf Area Variations

2.2.1 Declassified aerial photographs

The Antarctic Single Frame Record (ASFR) is a collection of aerial photographs dating from 1946 to 2000, which cover Antarctica and were provided by the United States Antarctic Resource Center and the British Antarctic Survey (BAS). The U.S. Navy began Antarctic flights with trimetrogon aerial photography (TMA) in 1946 and acquired >330,000 frames of photos. The U.S. Geological Survey (USGS) Earth Resources Observation and Science Center (EROS) declassified and released the ASFR digital files to the public domain.[27] In this study, we used >1500 aerial photographs collected along seven flight lines in 1968 (Table 1).

2.2.2 Satellite optical images

Earth Resources Technology Satellite (Landsat) imagery has been available since 1972.[28] The multispectral scanner (MSS) imagery from 1979 and the Thematic Mapper (TM) imagery from 1988 were employed to track the positions of the ice shelf front. Because of the constantly cloudy and snowy weather over the LIS, it is difficult to obtain continuous Landsat images with few or no clouds. Landsat data also suffer from low-temporal resolution. However, taking the availability and coverage frequency of the data into consideration, we employed MODIS imagery instead of Landsat imagery in 2000, 2009, and 2015, respectively. The MODIS data have been acquired by the US National Aeronautics and Space Administration (NASA) since February 2000.[29] To reduce errors resulting from different times, satellite images were ordered during the same season (austral summer) from 1979 to 2015, and the main observing period extended from January to March.

2.2.3 Processing of aerial photographs and satellite images

The aerial photos taken in 1968 were deformed before they were digitized. Therefore, they must be accurately orthorectified based on a new DEM by Cook et al.[24] Considering that the ASFR photos in 1968 had low geographic accuracy (they can provide only approximate latitude and longitude coordinates) and the MSS/MODIS images in 2000, 2009, and 2015 suffered from low spatial resolution, all of the orthorectified images listed in Table 1 and 2 were coregistered to the TM mosaic with high-quality features from 1988 (which were used as the common base images), using the feature-based method.[30] Then, ice shelves fronts in different years or extracted from different images could be mapped onto a common reference. The geolocation error of TM/ETM imagery is less than a half pixel, which is lower than that of MSS imagery (sometimes up to two pixels).[31] The geolocation uncertainty of MODIS imagery is 50 m at nadir.[32] However, after

Table 2 Landsat and MODIS images used for estimating extent changes in the LAIS and LBIS.

| Period	Date	Sensor	Resolution (m)	Path/row
1970s	February 01, 1979	MSS	57	231/105; 231/106; 231/107
	February 21, 1979	MSS	57	232/105; 232/106
1980s	February 12, 1988	TM	28.5	215/106
	February 19, 1988	TM	28.5	216/105; 216/106; 216/107
	March 01, 1988	TM	28.5	215/107
1990s	March 27, 2000, 13:15	MODIS	250	H14V15; H15V15
	March 29, 2000, 13:05	MODIS	250	H14V15; H15V15
2000s	April 8, 2009, 14:15	MODIS	250	H14V15; H15V15
2010s	March 28, 2015, 12:10	MODIS	250	H14V15; H15V15
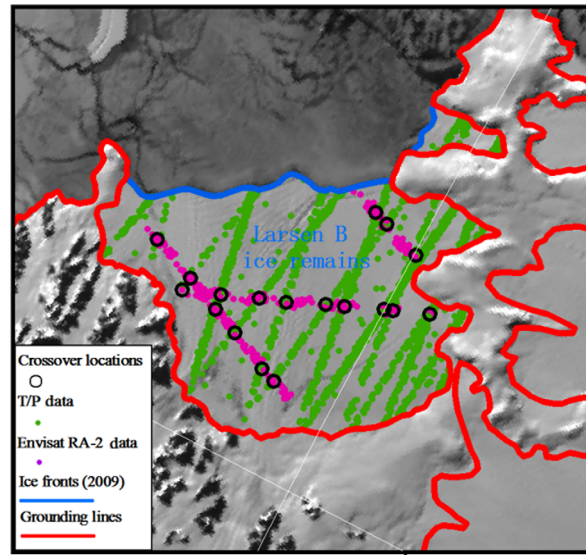
Fig. 2 The crossover locations over the remnant LBIS. The underlying image is a MODIS mosaic from 2009.

processing of the coregistered images, the registration accuracies image-to-image are within one pixel, corresponding to distances in the different images from ASFR, MSS, TM, and MODIS of ± 2.5, ± 57, ± 28.5, and ± 250 m, respectively.

The position of the ice shelf front was delineated once each decade. Thus, both the LAIS and the LBIS ice front positions were examined on six occasions. The ice front positions were manually digitized based on mosaics of the aerial photographs and MSS images assembled for the years 1968 and 1979, respectively. On the other hand, for the TM and MODIS images, we extracted the ice front positions automatically by image segmentation. Note that the ASFR flights in 1968 over the study area were conducted in austral spring months (September to December); thus, an abundance of sea ice occurred in the Weddell Sea. This feature led to a mosaic of the aerial photographs showing that sea ice abuts the floating ice shelf during this season [Fig. 3(a)]. For the dates when sea ice pixels were mixed with ice shelf pixels, locating the ice shelf front positions was much more difficult. Therefore, we delineated the ice shelf front position based on fractures and surface textures, and the delineation must be supplemented by a visual interpretation of the original images (ASFR photographs).

Grounding line extraction is another significant step in monitoring changes in ice shelves. A complete map of the high-resolution grounding lines for all of Antarctica has been generated based on a Radarsat image mosaic.[33] Thus, we extracted the grounding lines of the LAIS and the LBIS based on the existing database,[34,35] and we then used the grounding lines and ice front positions to delineate the boundaries of the ice shelves in different years. Once the boundaries were defined, the areas of the LAIS and the LBIS could be calculated.

2.3 *Radar Altimetry Data for Measuring Ice Shelf Elevation Variations*

2.3.1 *Satellite radar altimetry data*

The T/P satellite was launched on August 10, 1992. The Geophysical Data Record was the only altimeter on the satellite. The data from this sensor were continuously available from 1992 to 2005 and provided 479 cycles (003-481) of altimetry data. The orbit of the T/P was changed on September 15, 2002, and the repeat orbit was accordingly abandoned. Thus, the T/P data were used to cover the period of 1992 to 2001, which corresponds to cycles 009-364. The T/P data have a relatively large footprint of up to 3 to 4 km, and the along-track ground spacing is 5.96 km.[36] Envisat was launched on March 1, 2002, by the European Space Agency, and the Radar Altimeter-2 (RA-2) onboard Envisat is the first high-latitude (up to 82 deg) satellite
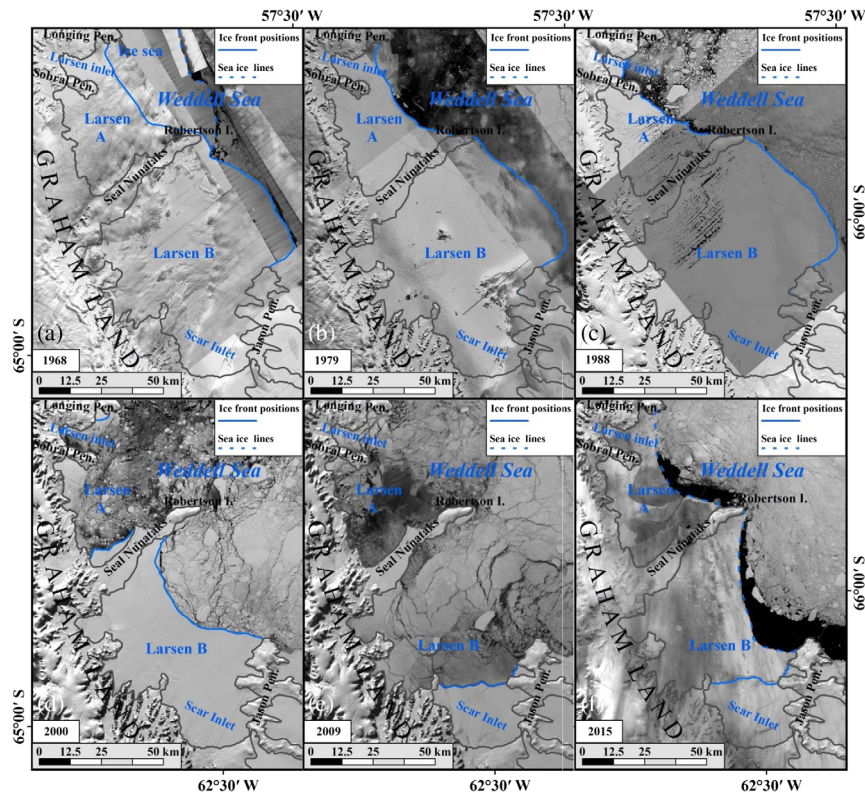
Fig. 3 (a) The image displaying the ice front in 1968 is a mosaic of ASFR aerial photographs, and the underlying images are a mosaic of MSS images in 1973. (b, c) The underlying images in 1979 and 1988 are mosaics of MSS images and TM images, respectively. (d–f) The underlying images in 2000, 2009, and 2015 are mosaics of MODIS images. The blue dashed lines indicate the sea ice extent in 1968 and 2015; the blue lines indicate ice front positions, and the gray lines indicate grounding lines.

altimeter.[37] The RA-2 provided 108 cycles (003-113) of altimetry data.[38] The orbit of Envisat was changed in October 2010.[39] Therefore, we selected the RA-2 data over the period from 2002 to 2010, which corresponds to cycles 006-094. The RA-2 data have a relatively large footprint size of 2 to 10 km and a relatively short along-track distance (370 m).[39]

2.3.2 *Processing of altimetry data*

The level-2 Envisat RA-2 data provide geolocated height estimates using the ICE-1 and ICE-2 waveform retrackers, respectively.[39] Many studies have shown that the ICE-2 algorithm provides the most accurate measurements of the ice caps.[40] Thus, the ICE-2 datasets are used in the present study. To maintain consistency with the Envisat level-2 product, the retracking process of the T/P data adopts the ICE-2 retracking algorithm.

WGS84/EGM96 is used for the RA-2 data,[38] whereas the T/P data employ a different reference system (i.e., the Topex/Poseidon ellipsoid system).[41] The elevation values from the T/P satellite were transformed with a constant height offset of 0.71 m that represents the difference between the ellipsoids of the T/P and WGS84 datums.[42] In addition, some important corrections of the geoid must be considered, including the ionospheric correction, the dry tropospheric correction, the wet tropospheric correction, the solid Earth tide correction, and the pole tide correction. The valid T/P data cover the period 1992 to 2002, whereas the valid RA-2 data cover the period 2002 to 2010. Thus, the existing data coincide in the same region (18 crossover locations over the study area) during the period between June and September 2002 (Fig. 2). We removed the systematic errors associated with the different satellites by comparing the coincident data at each crossover location during the same period.

Finally, the altimetry data need to be filtered based on normalization processing. Based on detailed observation of the normalization density distribution graphics, the thresholds of the elevation for selecting the T/P and RA-2 valid elevation points were set as 46.5 to 92.4 m and 45.6 to 91.1 m, respectively (the effective rates for T/P and RA-2 were 93.4% and 92.5%, respectively). Then, outliers were removed before the collinear analysis was performed.

2.4 Meteorological Data and Processing

To monitor the air-temperature changes over the northern LIS, the two research stations such as Marambio (64.23°S, 56.62°W, located on Marambio Island) and Matienzo (64.58°S, 60.04°W, located on Larsen Nunatak) were selected (Fig. 1). The mean annual and summer air temperatures measured at these stations over the past decades were employed. However, accurate precipitation is difficult to obtain at the research stations due to blowing-snow effects that can cause snow to be added to or removed from snow gauges once the wind speed exceeds ∼10 m/s.[43] Thus, we employed the Global Precipitation Climatology Project (GPCP) precipitation data for this study as the GPCP monthly products can provide consistent sources of global precipitation since 1980 by combining gauge observations, sounding observations, and various satellite precipitation data into 2.5-deg global grids.[44]

2.5 Error Analysis

The measurement uncertainty of the ice shelf front positions is limited by the image resolution and coregistration errors,[45] which can be assessed by the following equation:[46]

$$U_T = \sqrt{\sum \lambda^2} + \sqrt{\sum \varepsilon^2},\tag{1}$$

where U_T denotes the uncertainty in the ice shelf front positions, λ is the uncertainty in spatial resolution of images, and ε denotes the coregistration errors of each image to the 1988 TM mosaic.

The results indicate that the errors in ice shelf front positions derived from aerial photos, MSS, TM, and MODIS images are ±150, ±140, ±62, and ±260 m, respectively. However, considering that the LAIS and the LBIS cover relatively large areas, these uncertainties are acceptable for monitoring changes in the extents of these ice shelves on a large scale and over long periods of time.

To assess the uncertainty in ice elevations, we calculated the root mean square error (RMSE) of the altimetry crossover data by taking the difference between the ascending and descending observations within the same cycle.[22] After filtering the elevation data using normalization processing and removing outliers, the RMSE of the T/P and RA-2 crossover data was estimated to be ∼ ± 0.34 and ±0.19 m, respectively, within the study area when the data from all of the cycles were used. However, these uncertainties are still acceptable considering that the LAIS and the LBIS displayed high rates of elevation change, which are the elevations within the study area (which range from ∼40 to 90 m) are relatively high, and that the main purpose of this study is to reveal the overall temporal characteristics and change trends from the observed ice elevations.

3 Results

3.1 Retreat and Calving

As observed, the LAIS exhibited no significant changes from 1968 to 1986 when it merged with the Prince Gustav Ice Shelf at the Prince Gustav Channel [Fig. 3(a)]. From 1975 to 1986, the LAIS retreated by 540 km².[47] It began to retreat rapidly in 1987 [Fig. 3(c)], and the retreat culminated in a collapse in January to February 1995. The northern section of the LAIS disappeared almost completely from 1986 to 1997, and the area decreased by 2624 km².[48] The Larsen Inlet became disconnected from the LAIS, and very little ice remained during this period [Fig. 3(c)].

Additionally, the image mosaic from 2000 showed that very little ice remains in the LAIS [Fig. 3(d)], and it disappeared almost completely over the following several years [Fig. 3(e)].

The LBIS remained relatively stable until the early 1990s, and Figs. 3(a)–3(c) show small changes in the extent. However, it followed a pattern of retreat similar to that of the LAIS after the early 1990s, and it diminished by ∼1720 km^2 due to the calving event that took place in 1995.[48] A further decrease of ∼110 km^2 occurred due to calving in this section between February and March 1998; thus, the MODIS image mosaic for 2000 displays a major change in ice front positions compared with the earlier images [Fig. 3(d)]. The LBIS retreat culminated in a catastrophic collapse of ∼3250 km^2 in February 2002, and its area was subsequently only 20% of its earlier extent, consisting of ice held in Scar Inlet [Fig. 3(e)]. Obviously, the extent of the LBIS has tended to be more stable recently, and the area in 2015 displays a slight increase compared to that in 2009.

In summary, the total area of the LAIS and the LBIS has diminished by ∼14,000 km^2 since 1968, and the ice shelves within the study area have either retreated significantly or have been almost entirely lost (Figs. 4 and 5).
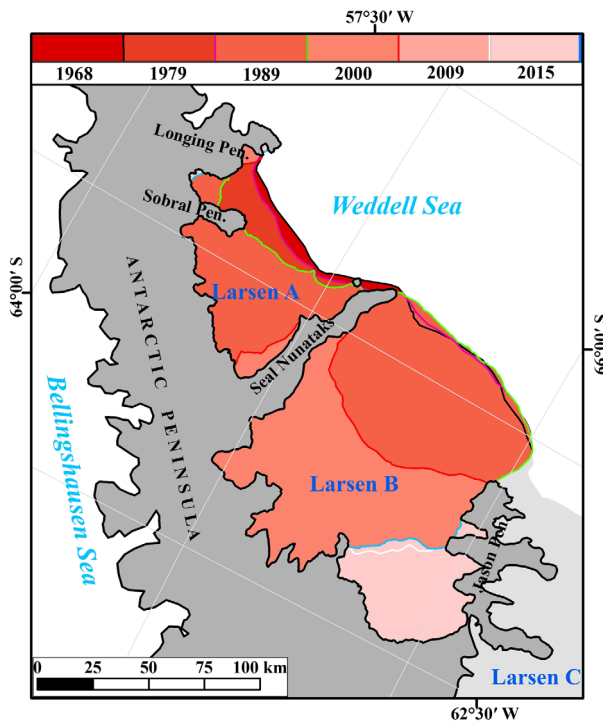

Fig. 4 The complete time series of the spatiotemporal changes in the LAIS and the LBIS over the past 48 years. The ice front positions in different years are marked as colored lines.
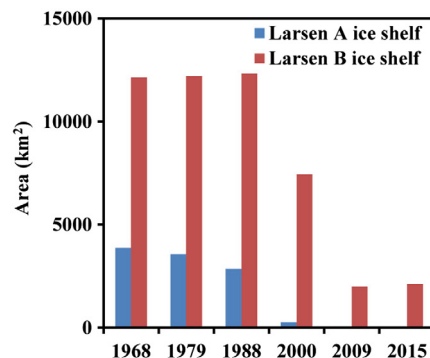

Fig. 5 Changes in the area of the LAIS and the LBIS from 1968 to 2015.

3.2 Progressive Thinning

The ice front positions varied remarkably in different years, and we monitored only the surface elevation of the floating ice. The minimum extent of the floating ice during the observation period is our focus. The northern part of the LIS experienced calving events in 1995 and 1998, and very little ice subsequently remained within the LAIS. In contrast, the LBIS still includes a relatively large area of ice shelf [Fig. 3(d)]. The remnant LBIS, which has an area of 2000 km^2, is located in Scar Inlet after a catastrophic collapse in 2002 [Fig. 3(e)]. Therefore, the elevation monitoring was divided into three groups: the remnant LAIS (1992 to 2001), the area near the front of the LBIS (1992 to 2001), and the remnant LBIS (1992 to 2010) (Fig. 6).

(1) The remnant LAIS: very little ice remained within the LAIS after 1995, and it disappeared completely in 2002. Thus, we monitored only the remnant LAIS, which has an area of 210 km^2, using the T/P data during the observing period from 1992 to 2001. The remnant LAIS showed progressive lowering; its elevation decreased at a rate of 0.45 m a^{-1} from 1992 to 2001. The elevation change curve displays two significant troughs (Fig. 7) that correspond to the calving event in 1995 and the near-total disappearance of the LAIS in 2000.

(2) The area near the front of the LBIS: we divided the LBIS into two monitoring areas (the remnant LBIS and the area near the front of the LBIS) (Fig. 6). The area near the front of the LBIS still existed after the calving events in 1995 and 1998, whereas it disappeared completely in 2002. Hence, the period was set to 1992 to 2001, and the T/P data were accordingly used. The area near the front of the LBIS had an area of 5440 km^2, and its lowering rate was significantly lower than that of the remnant LAIS (Fig. 7). The area near the front of the LBIS was lowered at a rate of 0.19 m a^{-1} from 1992 to 2001. Note that the elevation change curve of this region does not fluctuate markedly.

(3) The remnant LBIS: a dataset for the complete period was compiled by combining the T/P and RA-2 data (Fig. 6). The reduction rate of the remnant LBIS was significantly lower than those of the other two regions, and it displayed a lower rate of 0.07 m a^{-1} from 1992
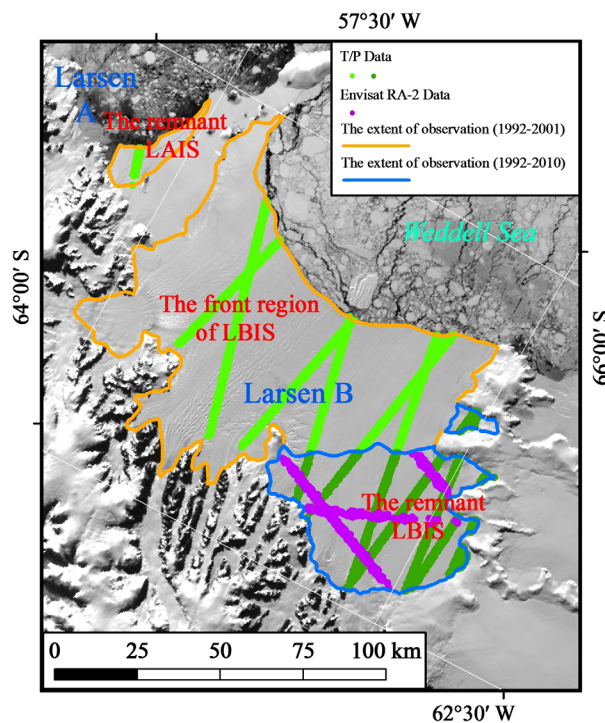

Fig. 6 Valid elevation locations are marked as colored dots. The T/P data from 1992 to 2001 are marked on the image in two different shades of green, and the RA-2 data from 2002 to 2010 are marked on the image in violet. The underlying image is a MODIS mosaic corresponding to 2000.
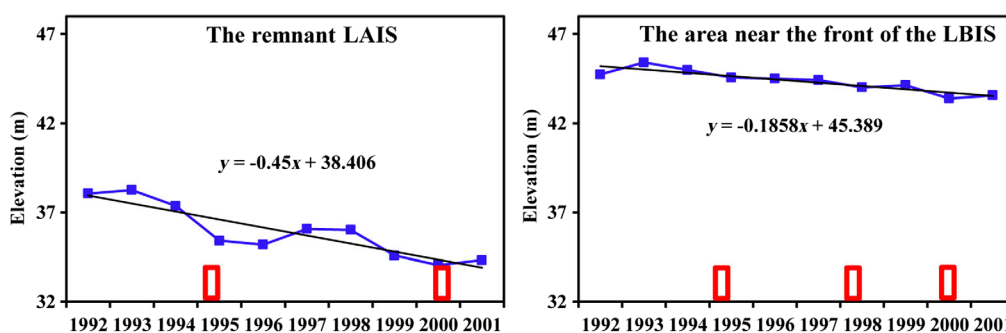
Fig. 7 Changes in surface elevations from 1992 to 2001 as recorded by the T/P radar altimeters. The blue lines indicate surface elevations in the remnant LAIS and the area near the front of the LBIS. The red rectangles in the left panel indicate the calving event of the LAIS in 1995 and the near-complete disappearance of the LAIS in 2000 to 2002. The red rectangles in the right panel indicate three calving events that took place in the LBIS in 1995, 1998, and 2002, respectively.

to 2010. We also found that the elevation change curve showed a large trough that was mainly related to the catastrophic collapse in February to March 2002. Additionally, there were several other troughs corresponding to calving events in 1995 and 1998, respectively. In line with our expectation, the surface elevation of the remnant LBIS tends to be more stable, corresponding to limited extent changes since 2002.

4 Discussion

One of the important mechanisms for thinning of the AP ice sheet is the increasing air temperature and the increased meltwater production and refreezing,[10] which leads to the lowering of the surface of the ice sheet. The ice shelves are more sensitive to atmospheric warming than the land ice of Antarctica is.[49] Therefore, warmer air temperatures have a profound effect on the surface mass balance of the LAIS and the LBIS. Atmospheric warming has led to longer melt seasons and an increase in melt pond extent.[5] Many dark patches can be seen on the TM/MODIS images collected after 1988 [Fig. 3(c)]. The summer air temperature at the Marambio station showed an obvious warming trend from 1986 to 1999 (Fig. 10). Therefore, with the aid of visual interpretation of the TM/MODIS images with few or no clouds, we can infer that an abundance of meltwater existed on the ice shelf surface as a result of the exceptionally warmer summers. In contrast to the strong warming trends observed during the second half of the 20th century, the northern AP shows much greater variability since 2000 and even displays a slight cooling trend.[50] The air-temperature changes in the northern LIS also coincide with this cooling trend, and the mean annual temperature trend at the Marambio station switched from a warming rate of 0.65°C ± 0.47°C per decade from 1971 to 2000 to a cooling rate of −1.46°C ± 2.4°C per decade from 2000 to 2010. In particular, the mean summer air temperatures at the Marambio and Matienzo stations showed obvious downward trends from 2000 to 2010 at average rates of −0.095°C a^{-1} and −0.081°C a^{-1}, respectively (Fig. 10). These temporal changes in air temperature may be related to the relative stability in the extent and surface elevation of the remnant LBIS in recent years (Figs. 4 and 8).

The surface mass balances of ice shelves are also profoundly impacted by precipitation over the entire embayment. We derived the annual mean precipitation over the Larsen A and B embayments from the GPCP monthly precipitation product. The results showed that the precipitation over the LAIS and the LBIS displayed an overall stable trend with several fluctuations from 1980 to 2010 (Fig. 9). It is worth noting that precipitation over the northern AP occurs mostly in summer.[51] Generally, an increase in the snow fall may offset the increased surface melt caused by atmospheric warming.[52] However, summer precipitation may fall as rain over the northern LIS, where weather is relatively warm and the summer air temperature is very close to or above 0°C (Fig. 10), resulting in decreased snow accumulation and increased extent of melt ponds over the past decades.
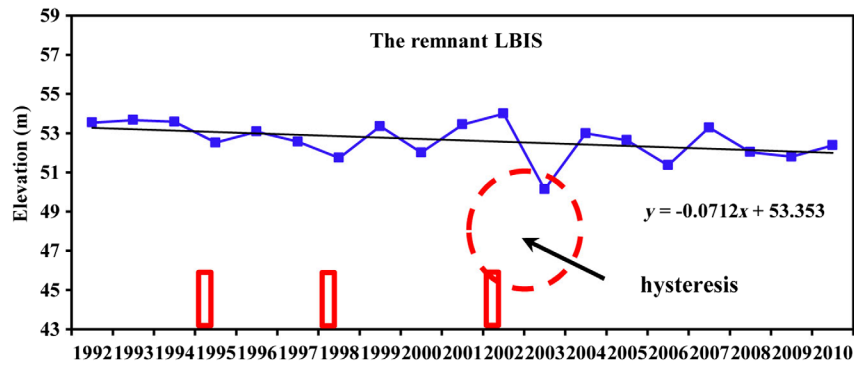
Fig. 8 Surface elevation changes recorded by the T/P and RA-2 radar altimeters and extracted using collinear analysis from 1992 to 2010. The red rectangles indicate the three calving events from the LBIS that occurred in 1995, 1998, and 2002, respectively.
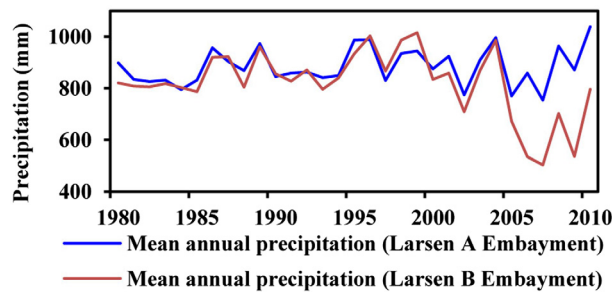

Fig. 9 Changes in mean annual precipitation over the Larsen A and B embayments from 1980 to 2010.
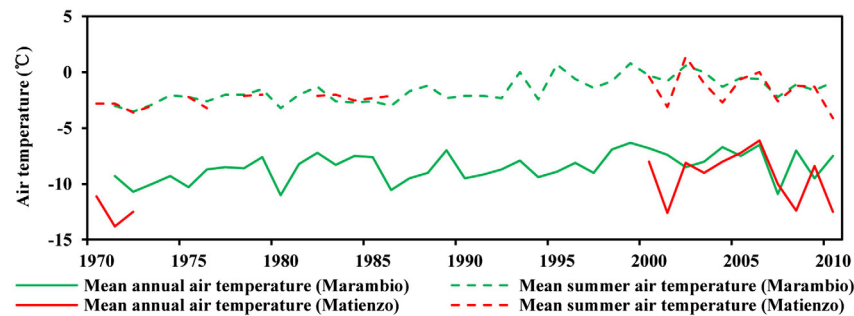

Fig. 10 Mean annual and summer air temperature records at two research stations within the northern LIS. The red dashed but discontinuous lines indicate incomplete temperature records at the Matienzo station.

The very small positive correlation coefficient between the mean summer air temperature and the surface elevation of the LBIS from 2000 to 2010 indicates that the covariation is very weak if it exists (Fig. 11). Furthermore, the even smaller correlation coefficient between the mean annual precipitation and the surface elevation indicates that their covariation is insignificant. These results are beyond our expectation and may be partly caused by ice shelf retreat and disintegration. Through a detailed analysis of the relationships between the surface elevation and air temperature/precipitation (Fig. 11), we infer that the surface mass balances of the LAIS and the LBIS are not appreciably impacted by the air temperature and precipitation during the observing period. Compared with the drastic elevation loss of the northern LIS, possibly due to ice calving, these impacts seem to be limited.
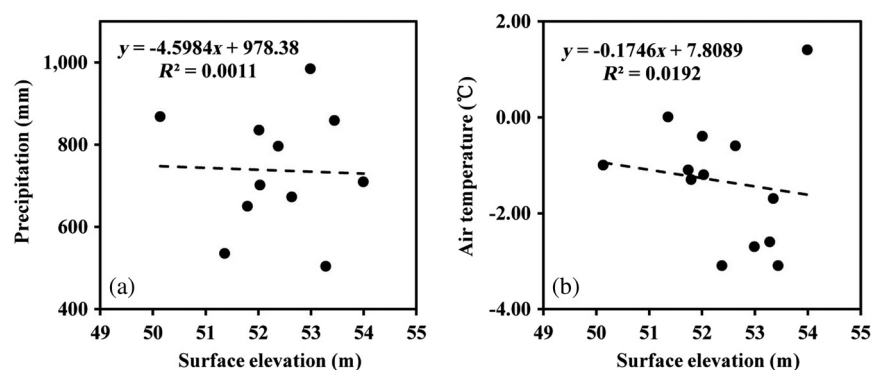
Fig. 11 The relationships between the surface elevation of the LBIS and (a) mean annual precipitation and (b) summer air temperatures at the Matienzo station from 2000 to 2010.

Ice shelves can create a backward pressure, blocking the downward flow of ice from grounded glaciers.[53] This restrictive longitudinal stress decreases when ice shelves collapse or retreat, causing faster flow and increased ice discharge. Thus, as shown in Figs. 7 and 8, there is a one-to-one correspondence between significant troughs in the elevation curves and the calving events. On the other hand, the ice shelf fronts tended to be more stable in the years after large calving events occurred, and a more stable ice discharge system created a greater backward pressure to block ice discharge. On this basis, with increasingly more ice discharge from grounded glaciers into downstream ice shelves, the surface elevation can recover from the elevation loss caused by large calving events (Fig. 8). It is worth pointing out that the ice shelf thinning does not appear to be related only to calving events; the reductions in ice elevation show a small degree of hysteresis behavior (e.g., Fig. 8 shows a catastrophic collapse in February to March 2002, whereas a large trough corresponds to the period from late 2002 to 2003). This hysteresis provides further evidence that ice retreat leads to a reduction in backstress, resulting in increased ice discharge and dramatic elevation decrease. Based on the above analysis and the low correlation coefficients between the surface elevation and air temperature ($R^2 = 0.019$) and precipitation ($R^2 = 0.001$), we conclude that in response to the continuous retreat of the LAIS and the LBIS, their average surface elevations are more sensitive to the collapse and retreat of the ice shelf than to the changes in air temperature and precipitation.

5 Conclusion

We compiled a 48-year time series of monitoring data for studying the retreat of the LAIS and the LBIS by combining declassified aerial photographs and satellite optical images. In addition, we assessed the variations in the surface elevation of the LAIS and the LBIS from 1992 to 2010 by applying the collinear analysis method to satellite radar altimetry data (T/P and RA-2). The results showed that the LAIS and the LBIS began to retreat gradually in the 1980s in response to atmospheric warming. The LAIS and the LBIS diminished by ~14,000 km² in total area from 1968 to 2015. At the same time, the LAIS and the LBIS displayed progressive lowering in recent decades, although the rate of reduction of the LAIS was significantly greater than that of the LBIS. The remnant LAIS was lowered at a rate of 0.45 m a^{-1} from 1992 to 2001, and the remnant LBIS was lowered at a rate of 0.07 m a^{-1} from 1992 to 2010. In response to the continuous retreat of the LAIS and the LBIS, their surface elevations were very sensitive to the collapse and retreat of the ice shelves. The calving and retreat of the ice shelves led to a reduction in backstress, increased ice discharge, and dramatic elevation decrease. In summary, the variations in ice shelf extent and ice shelf surface elevation profoundly affected the surface mass balances of the LAIS and the LBIS.

The LIS is closely connected to both the surrounding ocean and the atmosphere.[9] Factors that can impact the surface mass balance include precipitation, surface meltwater production and refreezing, and iceberg calving. Furthermore, the increased basal melting that is caused by ocean warming can exert an important control on the basal mass balance of ice shelves.

We excluded basal mass balance from the detailed analysis presented in this paper, due to the lack of deep-sea temperature data and ice thickness data.

Acknowledgments

References

1. B. K. Lucchitta and C. E. Rosanova, "Velocities of Pine Island and Thwaites Glaciers, West Antarctica, from ERS-1 SAR images," in *European Space Agency, (Special Publication) ESA SP*, pp. 819–824 (1997).

2. Y. Cai, C. Q. Ke, and Z. Duan, "Monitoring ice variations in Qinghai Lake from 1979 to 2016 using passive Microwave remote sensing data," *Sci. Total Environ.* **607**–**608**, 120–131 (2017).

3. J. Chen et al., "Surface velocity estimations of ice shelves in the northern Antarctic Peninsula derived from MODIS data," *J. Geogr. Sci.* **26**(2), 243–256 (2016).

4. P. Skvarca et al., "Climatic trend and the retreat and disintegration of ice shelves on the Antarctic Peninsula: an overview," *Polar Res.* **18**(2), 151–157 (2010).

5. M. A. Fahnestock, W. Abdalati, and C. A. Shuman, "Long melt seasons on ice shelves of the Antarctic Peninsula: an analysis using satellite-based microwave emission measurements," *Ann. Glaciol.* **34**(1), 127–133 (2002).

6. A. Shepherd et al., "Larsen ice shelf has progressively thinned," *Science* **302**(5646), 856–859 (2003).

7. D. G. Vaughan and C. S. M. Doake, "Recent atmospheric warming and retreat of ice shelves on the Antarctic Peninsula," *Nature* **379**(6563), 328–331 (1996).

8. S. Christopher, T. A. Scambos, and B. Etienne, "Ice loss processes in the Seal Nunataks ice shelf region from satellite altimetry and imagery," *Ann. Glaciol.* **57**(73), 94–104 (2016).

9. A. E. Hogg and G. H. Gudmundsson, "Impacts of the Larsen-C Ice Shelf calving event," *Nat. Clim. Change* **7**, 540–542 (2017).

10. H. A. Fricker and L. Padman, "Thirty years of elevation change on Antarctic Peninsula ice shelves from multimission satellite radar altimetry," *J. Geophys. Res.* **117**(C2), 73 (2012).

11. C. A. Shuman, E. Berthier, and T. A. Scambos, "2001–2009 elevation and mass losses in the Larsen A and B embayments, Antarctic Peninsula," *J. Glaciol.* **57**(204), 737–754 (2011).

12. T. Heid and A. Kääb, "Evaluation of existing image matching methods for deriving glacier surface displacements globally from optical satellite imagery," *Remote Sens. Environ.* **118**(118), 339–355 (2012).

13. H. Rott, P. Skvarca, and T. Nagler, "Rapid collapse of Northern Larsen Ice Shelf, Antarctica," *Science* **271**(5250), 788–792 (1996).

14. B. K. Lucchitta and C. E. Rosanova, "Retreat of northern margins of George VI and Wilkins Ice Shelves, Antarctic Peninsula," *Ann. Glaciol.* **27**, 41–46 (1998).

15. T. A. Scambos et al., "Detailed ice loss pattern in the northern Antarctic Peninsula: widespread decline driven by ice front retreats," *Cryosphere* **8**(6), 2135–2145 (2014).

16. E. Berthier, T. A. Scambos, and C. A. Shuman, "Mass loss of Larsen B tributary glaciers (Antarctic Peninsula) unabated since 2002," *Geophys. Res. Lett.* **39**, L13501 (2012).

17. A. Shepherd et al., "A reconciled estimate of ice-sheet mass balance," *Science* **338**(6111), 1183–1189 (2012).

18. I. Sasgen et al., "Timing and origin of recent regional ice-mass loss in Greenland," *Earth. Planet. Sci. Lett.* **333**–**334**(6), 293–303 (2012).

19. T. Haug, A. Kääb, and P. Skvarca, "Monitoring ice shelf velocities from repeat MODIS and Landsat data—a method study on the Larsen C ice shelf, Antarctic Peninsula and 10 other ice shelves around Antarctica," *Cryosphere* **4**(2), 161–178 (2010).

20. D. C. Slobbe, P. Ditmar, and R. C. Lindenbergh, "Estimating the rates of mass change, ice volume change and snow volume change in Greenland from ICESat and GRACE data," *J. Roy. Astron. Soc.* **176**(1), 95–106 (2009).

21. M. A. King et al., "A 4-decade record of elevation change of the Amery Ice Shelf, East Antarctica," *J. Geophys. Res.* **114**(114), 436–448 (2009).

22. H. Lee et al., "Elevation changes of Bering Glacier System, Alaska, from 1992 to 2010, observed by satellite radar altimetry," *Remote Sens. Environ* **132**(10), 40–48 (2013).

23. A. Kääb et al., "Contrasting patterns of early twenty-first-century glacier mass change in the Himalayas," *Nature* **488**(7412), 495–498 (2012).

24. A. J. Cook et al., "A new 100-m Digital Elevation Model of the Antarctic Peninsula derived from ASTER Global DEM: methods and accuracy assessment," *Earth Syst. Sci. Data* **4**(1), 129–142 (2012).

25. J. A. Griggs and J. L. Bamber, "Ice shelf thickness over Larsen C, Antarctica, derived from satellite altimetry," *Geophys. Res. Lett.* **36**(19), 308–308 (2009).

26. T. Haran, *MODIS Mosaic of Antarctica (MOA) Image Map, Digital Media*, National Snow and Ice Data Center, Boulder, Colorodo (2006).

27. ASFR, "Polar Geospatial Center," http://applications.pgc.umn.edu/flash/tma/ (December 2015).

28. USGS, "USGS Center for Earth Resources Observation and Science," http://earthexplorer.usgs.gov/ (November 2015).

29. EOSDIS, "The Earth Observing System Data and Information System," https://ladsweb.modaps.eosdis.nasa.gov/ (November 2016).

30. B. Zitová and J. Flusser, "Image registration methods: a survey," *Image Vision Comput.* **21**(11), 977–1000 (2003).

31. T. He et al., "Evaluating land surface Albedo estimation from Landsat MSS, TM, ETM +, and OLI data based on the unified direct estimation approach," *Remote Sens. Environ.* **204**, 181–196 (2018).

32. R. E. Wolfe et al., "Achieving sub-pixel geolocation accuracy in support of MODIS land science," *Remote Sens. Environ.* **83**, 31–49 (2002).

33. H. X. Liu and K. C. Jezek, "A complete high-resolution coastline of Antarctica extracted from orthorectified radarsat SAR Imagery," *Photogramm. Eng. Remote Sens.* **70**(5), 605–616 (2004).

34. A. Khazendar et al., "The evolving instability of the remnant Larsen B Ice Shelf and its tributary glaciers," *Earth Planet. Sci. Lett.* **419**, 199–210 (2015).

35. E. Rignot, J. Mouginot, and B. Scheuchl, "Antarctic grounding line mapping from differential satellite radar interferometry," *Geophys. Res. Lett.* **38**(10), L10504 (2011).

36. A. V. Kouraev et al., "Ob' river discharge from TOPEX/Poseidon satellite altimetry (1992–2002)," *Remote Sens. Environ.* **93**(1–2), 238–245 (2004).

37. M. Roca, S. Laxon, and C. Zelli, "The EnviSat RA-2 instrument design and tracking performance," *IEEE Trans. Geosci. Remote Sens.* **47**(10), 3489–3506 (2009).

38. S. Batoula et al., "Envisat altimetry level 2 user manual," Issue 1:4 (2011).

39. L. S. Sørensen et al., "Envisat-derived elevation changes of the Greenland ice sheet and a comparison with ICEsat results in the accumulation area," *Remote Sens. Environ.* **160**, 56–62 (2015).

40. B. Legresy et al., "ENVISAT radar altimeter measurements over continental surfaces and ice caps using the ICE-2 retracking algorithm," *Remote Sens. Environ.* **95**(2), 150–163 (2005).

41. J. J. Zheng et al., "Monitoring changes in the water volume of Hulun Lake by integrating satellite altimetry data and Landsat images between 1992 and 2010," *J. Appl. Remote Sens.* **10**(1), 016029 (2016).

42. G. Le, J. J. Liao, and G. Z. Shen, "Monitoring lake-level changes in the Qinghai–Tibetan Plateau using radar altimeter data (2002–2012)," *J. Appl. Remote Sens.* **7**(21), 073470 (2013).

43. J. Turner et al., "Antarctic climate change during the last 50 years," *Int. J. Climatol.* **25**(3), 279–294 (2005).

44. R. F. Adler et al., "The version-2 global precipitation climatology project (GPCP) monthly precipitation analysis (1979 present)," *J. Hydrometeorol.* **4**(6), 1147 (2003).

45. D. K. Hall et al., "Consideration of the errors inherent in mapping historical glacier positions in Austria from ground and space (1893-2001)," *Remote Sens. Environ.* **86**(4), 566–577 (2003).
46. Q. Ye et al., "Monitoring glacier variations on Geladandong mountain, central Tibetan Plateau, from 1969 to 2002 using remote-sensing and GIS technologies," *J. Glaciol.* **52**(179), 537–545 (2006).
47. P. Skvarca, "Fast recession of the northern Larsen Ice Shelf monitored by space images," *Ann. Glaciol.* **17**, 317–321 (1993).
48. H. Rott et al., "Climatically induced retreat and collapse of northern Larsen Ice Shelf, Antarctic Peninsula," *Ann. Glaciol.* **27**, 86–92 (1998).
49. D. G. Vaughan, "Recent trends in melting conditions on the Antarctic Peninsula and their implications for ice-sheet mass balance and sea level," *Arct. Antarct. Alp. Res.* **38**(1), 147–152 (2006).
50. D. J. Mcgrath, *Basal Crevasses and Suture Zones in the Larsen C Ice Shelf, Antarctica: Implications for Ice Shelf Stability in a Warming Climate*, University of Colorado (2013).
51. J. Turner et al., "A positive trend in western Antarctic Peninsula precipitation over the last 50 years reflecting regional and Antarctic-wide atmospheric circulation changes," *Ann. Glaciol.* **41**(1), 85–91 (2005).
52. N. E. Barrand et al., "Computing the volume response of the Antarctic Peninsula ice sheet to warming scenarios to 2200," *J. Glaciol.* **59**(59), 397–409 (2013).
53. E. Rignot et al., "Accelerated ice discharge from the Antarctic Peninsula following the collapse of Larsen B ice shelf," *Geophys. Res. Lett.* **31**(18), L18401 (2004).

Jun Chen is a senior engineer at Anhui Jianzhu University. He received his PhD from Nanjing University in 2016. His current research interests include new techniques and applications for geography information systems, land use classification, eco-environment quality evaluation, and environmental remote sensing.

Biographies for the other authors are not available.